Available online at www.sciencedirect.com

ScienceDirect

Ceramics International 40 (2014) 2179–2186

CERAMICS INTERNATIONAL

www.elsevier.com/locate/ceramint

Structural, morphological and gas sensing properties of undoped and Lanthanum doped nanocrystalline SnO_2

L.P. Chikhale[a], J.Y. Patil[a], A.V. Rajgure[a], F.I. Shaikh[a], I.S. Mulla[b], S.S. Suryavanshi[a,*]

[a]School of Physical Sciences, Solapur University, Solapur 413255, India
[b]Emeritus Scientist (CSIR), Centre for Materials for Electronic Technology (C-MET), Pune 411008, India

Received 6 July 2013; received in revised form 28 July 2013; accepted 28 July 2013
Available online 7 August 2013

Abstract

Undoped and Lanthanum doped tin dioxide nanopowders were successfully synthesized by a chemical co-precipitation method. The TGA–DTA, XRD, TEM, SEM, EDAX, FTIR, Raman and UV–vis techniques were used to characterize various physico-chemical properties of samples. Thick films of functional material were prepared by using a screen printing technique and then sintered at 650 °C for 2 h. XRD analysis of all the samples revealed formation of single phase rutile type tetragonal structures which was further supported by Raman studies and FTIR measurements. The particle size of sintered SnO_2 was decreased with La doping, confirming the role of La as a grain growth inhibitor. Morphological studies revealed formation of porous structure useful for gas sensing application. Gas sensing characteristics were investigated towards various reducing gases such as liquefied petroleum gas (LPG), acetone (CH_3COCH_3), ethanol (C_2H_5OH) and ammonia (NH_3). The maximum response was exhibited by 3 mol% La doped SnO_2 thick film towards acetone vapor at an operating temperature of 300 °C. The sensor exhibited quick response and recovery times which were 20 s and 48 s, respectively.

Keywords: Tin oxide; Thick film; Gas sensor; Sensitivity; XRD

1. Introduction

Nanostructured semiconductor oxides are attracting a great deal of attention due to their exclusive properties and novel applications. Semiconductor gas sensors based on metal oxides have been used to detect toxic and inflammable gases. These gas sensing materials include semiconductor oxides such as SnO_2, ZnO, In_2O_3, TiO_2 and Fe_2O_3. They offer potential for developing portable and economical gas sensing devices due to their simplicity, high sensitivity and fast response.

Among these materials SnO_2 has been employed for detection of numerous gases [4]; however pristine SnO_2 possesses poor selectivity and high working temperatures. It is a promising multifunctional material with excellent properties such as high degree of transparency in the visible spectrum, strong physical and chemical interaction with adsorbed species and strong thermal stability [1–3]. Introduction of dopants in the host material is the most commonly adopted way to modify the characteristics of a sensor material. Several researchers have reported the influence of different dopants on the structural, morphological and gas response properties of tin dioxide based sensors [5–10]. A variety of methods have been utilized for the synthesis of SnO_2 which includes hydrothermal method [11], spray pyrolysis technique [12], sol–gel methods [13], co-precipitation [14], solid state route [15], chemical vapor deposition [16], etc. Amongst these, the co-precipitation method has advantages like low temperature processing, facile and molecular level homogeneity.

To the best of our knowledge, there are no reports on the effect of La doping on gas sensing properties of SnO_2 synthesized by co-precipitation route. Lanthanum is a catalytically active material and has been reported to be a promising promoter for SnO_2 based gas sensors [17,18]. It is well known that the gas sensing properties of semiconductor metal oxides are strongly related to their acid/base characteristics. SnO_2 is a predominantly acidic oxide, while the rare earth oxide La_2O_3 is basic. The Lanthanum doping is expected to enhance the gas response properties of SnO_2 based sensor. In the present study, we report structural, morphological, optical and gas response properties of the undoped and La doped SnO_2.

*Corresponding author. Tel.: +91 217 2744771; fax: +91 217 2744770.
E-mail address: sssuryavanshi@rediffmail.com (S.S. Suryavanshi).

0272-8842/$ - see front matter © 2013 Elsevier Ltd and Techna Group S.r.l. All rights reserved.
http://dx.doi.org/10.1016/j.ceramint.2013.07.136

2. Experimental procedure

2.1. Preparation of undoped and doped SnO_2 nanocrystalline powder

Undoped and La doped SnO_2 nanopowders were synthesized by a simple co-precipitation route. The starting precursors used were tin(IV) chloride pentahydrate ($SnCl_4 \cdot 5H_2O$, analytical grade), lanthanum nitrate ($La(NO_3)_3 \cdot 5H_2O$) and ammonia ($NH_3 \cdot H_2O$, analytical grade). Tin chloride was dissolved in distilled water to form a transparent solution. Then to this resulting solution, ammonia was added drop-wise under magnetic stirring until pH > 8 where the precipitation was formed. The obtained precipitate was washed for several times with de-ionized water and further dried under IR lamp for 2 h. The dried precipitate powder was calcined at 450 °C for 2 h in muffle furnace (this sample was labeled as C1). In a similar way, SnO_2 with different La dopings (1, 3 and 5 mol%) were prepared. The composition and nomenclature of samples synthesized in this study are given in Table 1.

2.2. Deposition of thick films

The thixotropic paste was made by mixing the fine SnO_2 calcined powder with a mixture of ethyl cellulose (a temporary binder), butyl carbitol acetate and terpineol. The ratio of inorganic to organic part was kept at 75:25 [19]. This paste was deposited on to the ultrasonically cleaned alumina substrate (10 mm × 20 mm) by using a screen printing technique having nylon cloth screen of 140 mesh counts. The details of the technique are described elsewhere [20]. The thick films were further sintered at 650 °C for 2 h in the muffle furnace.

2.3. Characterization

The as-synthesized precipitate was subjected to thermogravimetric–differential thermal analysis (TG–DTA) to study the phase formation temperature. The TG–DTA was recorded on the SDT Q 600 V20.9 Build20 instrument, in air atmosphere from room temperature to 1000 °C with a heating rate of 10 °C/min.

The X-ray diffraction (XRD) patterns of various samples were obtained using a BRUKER AXS D8-Advanced X-ray diffractometer using Cu-Kα ($\lambda = 1.54$ Å) radiation for 2θ value in the range 20–80°. The average crystallite size (D) of undoped and La doped SnO_2 sintered powder was estimated by using the Scherrer equation as follows:

$$D = \frac{0.9\lambda}{\beta \text{Cos } \theta} \quad (1)$$

Table 1
Sample identification for SnO_2.

Sample code	Composition
C1	Undoped SnO_2
C2	99 mol% $SnCl_4$+1 mol% $La(NO_3)_3$
C3	97 mol% $SnCl_4$+3 mol% $La(NO_3)_3$
C4	95 mol% $SnCl_4$+5 mol% $La(NO_3)_3$

where, λ, β and θ are X-ray wavelength, full width at half maximum (FWHM) of the most intense diffraction peak and the Braggs diffraction angle respectively.

Scanning electron microscope (SEM; model JSM-6360) was used to examine the surface morphology of sintered samples and the energy dispersive X-ray (EDAX) technique was used to determine their elemental compositions.

Transmission electron microscope (TEM) images were taken by using a Philips CM 200 FEG microscope equipped with a field emission gun at an accelerating voltage of 200 kV and having a resolution of 0.24 nm.

The UV-absorption spectra of undoped and La doped SnO_2 were recorded on a JASCO (model V-670) UV–vis–NIR spectrophotometer. The spectra were taken in the wavelength range of 200–1000 nm and further utilized for determining the optical band gap.

FTIR spectroscopic measurements of the sintered samples were taken in the wave number range of 400–4000 cm^{-1}, on a JASCO Model FTIR-6100 type spectrophotometer to study the chemical groups present in the samples.

The Raman spectra of SnO_2 thick films doped with different La concentrations were taken at room temperature in back-scattering geometry using a Thermo Fisher DXR Raman spectrometer with semiconductor laser beam having the excitation wavelength of 532 nm.

2.4. Gas response measurement

The gas sensing properties of undoped and La doped SnO_2 thick film were studied in an indigenously developed gas sensor set-up comprising of a controlled temperature furnace and a gas chamber (1 L volume). The temperature of the system was controlled from room temperature to 500 (±2) °C. Digital Nanometer (model DNM-121) and Scien Tech variable power supply ST4074 were used to measure the resistance of sample. Conducting silver paste was used to form ohmic contacts (1 mm) on the thick film sample. The sensor response (S) to a reducing gas was calculated using the equation:

$$S(\%) = \frac{(R_a - R_g)}{R_a} \times 100 \quad (2)$$

where R_a and R_g are the resistance of sensor in air and in presence of test gas respectively.

3. Results and discussion

3.1. TGA–DTA analysis

Fig. 1 shows the TG–DTA curves of the 3 mol% La-doped SnO_2 precipitate powder. The TGA curve shows a gradual decrease in weight with temperature up to 600 °C. The DTA curve shows a weak endothermic peak at around 100 °C and a broad exothermic peak in the range 200–300 °C. The decrease in weight in TGA curve and an endothermic peak around 100 °C in DTA curve corresponds to the removal of hydroxide ions. Further decrease in weight and exothermic peak in the range 200–300 °C can be attributed to the recrystallization and

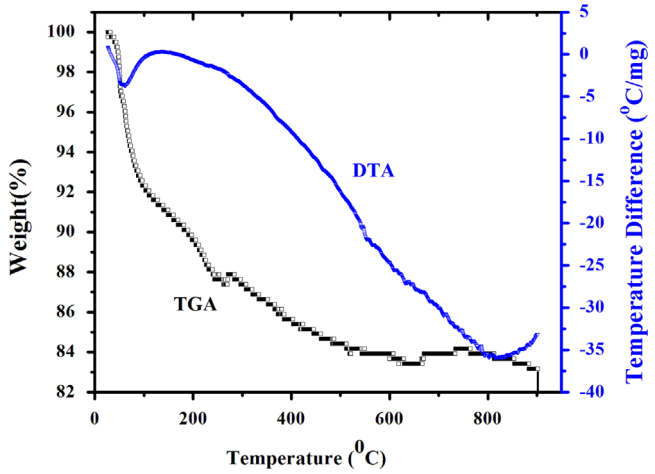

Fig. 1. TGA–DTA profile of the precipitate precursor of 3 mol% La doped SnO_2.

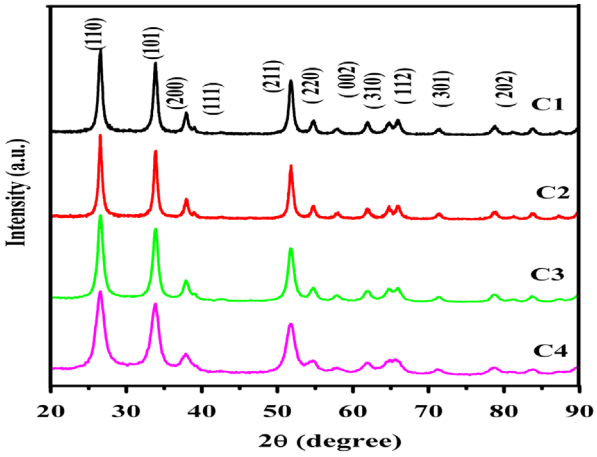

Fig. 2. XRD patterns of SnO_2 sintered powder: (C1) undoped SnO_2, (C2) 1 mol% La doped, (C3) 3 mol% La doped, and (C4) 5 mol% La doped SnO_2.

Table 2
Average particle size and lattice parameters of undoped and La-doped SnO_2.

Sample code	Average crystallite size (nm) from XRD	Average particle size (nm) from TEM	Lattice parameter a (Å)	c (Å)	Band gap (eV)
C1	14	15	0.4746	0.3188	3.23
C2	10	11	0.4748	0.3192	2.88
C3	7	7	0.4751	0.3198	2.70
C4	5	5	0.4758	0.3201	2.59

oxidation of precipitate powder. We do not observe any weight loss beyond 600 °C indicating complete phase formation of the material. In accordance with TG–DTA studies we have selected 650 °C as a sintering temperature.

3.2. XRD analysis

Fig. 2 shows the XRD patterns of undoped and La doped SnO_2 powders sintered at 650 °C. All the diffraction peaks were indexed to the tetragonal rutile structure of SnO_2 (JCPDS no. 41-1445) with the maximum intensity peak corresponding to (110) planes. Absence of peaks corresponding to any other phase confirms the substitution of La in SnO_2 crystal. The lattice parameters and average crystallite size for various SnO_2 samples are given in Table 2.

The lattice parameters of the undoped SnO_2 are in good agreement with the reported value in JCPDS no. 41-1445. The lattice parameters were slightly increased with La doping which can be attributed to its larger ionic radius (101 pm) as compared to that of Sn (71 pm) ions [21]. The average crystallite size was decreased with La doping which is clearly seen through broadening and lowering of intensity of the intense peak. The decrease in the crystallite size with La doping is in good agreement with the earlier reports [22].

3.3. Scanning electron microscopy and energy dispersive X-ray analysis

Fig. 3 shows SEM images of sintered thick films of undoped and La doped SnO_2. All the micrographs show porous microstructure with non-uniformly distributed pores (void) on the surface. This porous morphology is helpful for gas sensing, as it provides more surface area for adsorption of oxygen and its reaction with the relevant test gas. The EDAX spectrum of 3 mol% La doped SnO_2 (C3) is shown in Fig. 4. It shows presence of peaks corresponding to lanthanum, tin and oxygen. The EDAX data in Table 3 confirms presence of these elements as per the initial ratio.

3.4. Transmission electron microscopy (TEM) analysis

Fig. 5 shows TEM images of undoped and La doped SnO_2 thick film samples. It shows agglomeration of fine nanoparticles in all samples. This agglomeration is supposed to be due to the superposition and junction of particles. The crystallite size from TEM analysis matches well with XRD results confirming the usefulness of co-precipitation route for the synthesis of nanocrystalline material. The selected area electron diffraction (SAED) pattern (shown in inset) of an isolated particle exhibits bright rings which corresponds to the lattice planes of SnO_2.

3.5. Optical studies

The plot of $(\alpha h\nu)^2$ as a function of the energy ($h\nu$) of the incident radiation for undoped and La doped SnO_2 samples is shown in Fig. 6. All plots show nonlinear nature, which indicates direct transition nature. The band gap was evaluated from the intercept of extrapolated linear part of curve on the energy axis. The band gap energy was evaluated from absorption edge corresponding to the relation [23]:

$$\alpha = \text{const} \times \frac{(h\nu - E_g)^{1/2}}{h\nu} \quad (3)$$

where E_g is the optical band gap energy calculated from $(\alpha h\nu)^2$ versus energy ($h\nu$) plot, α is the absorption coefficient, $h\nu$ is the photon energy taken from the UV-spectra. The band edge can be evaluated from the intercept of the extrapolated linear

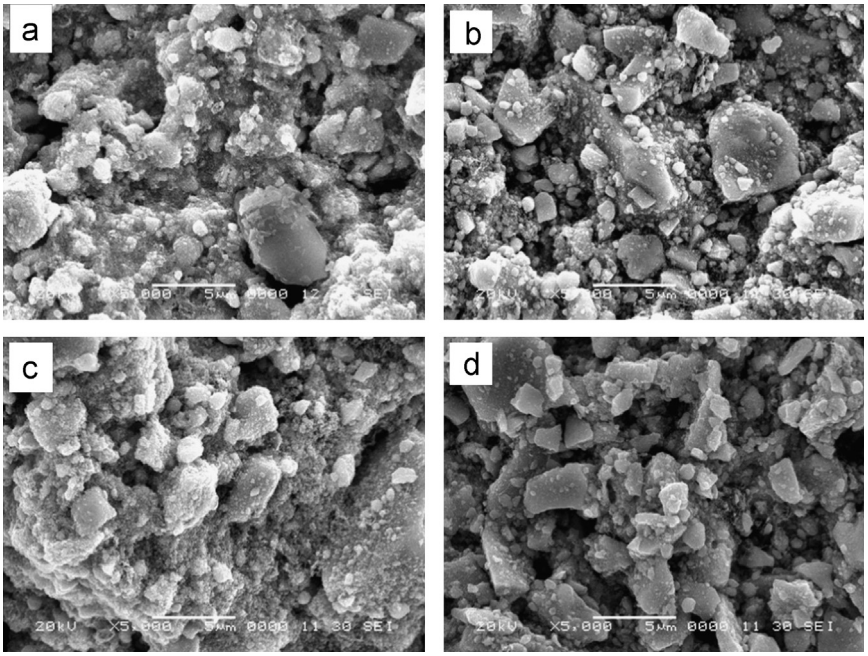

Fig. 3. SEM images of SnO_2 thick films: (a) undoped SnO_2, (b) 1 mol% La doped SnO_2, (c) 3 mol% La doped and (d) 5 mol% La doped SnO_2.

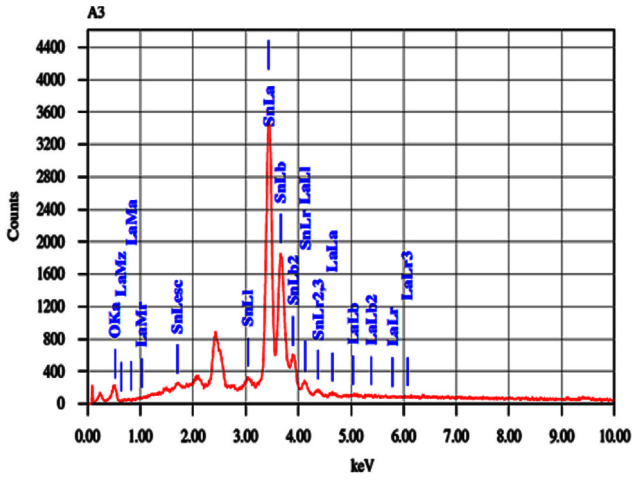

Fig. 4. EDAX spectrum of 3 mol% La doped SnO_2 thick film.

Table 3
Element concentrations calculated from energy dispersive X-ray spectroscopy (EDAX) of 3 mol% La-doped SnO_2.

Element	Wt%	At%
La	1.84	0.91
Sn	86.76	50.16
O	11.41	48.93

part of the curve on energy axis. The corresponding value of optical band gap (E_g) for undoped SnO_2 was 3.25 eV while 2.88, 2.70, 2.59 eV for 1, 3 and 5 mol% La doped SnO_2 (Table 2) respectively.

The observed decrease in band gap with addition of La is analogous to studies reported earlier [24]. The decrease in band gap was reflected by the red shift in absorption spectra to a certain minimum value. The shift in band-gap with the doping of La is attributed to the change in energy eigen value result by perturbation potential caused by the exchange interaction. The variation in band gap due to doping can be a result of Mosse–Burstein (MB) effect, in which the band gap can be presented as $E_g = E_{go} + \Delta E_{MB}$, where E_{go} is the intrinsic band gap and ΔE_{MB} is the amount of band gap change (a function of electron or hole concentration) [25]. The other reason for optical band gap reduction may be the appearance of the La–Sn metallic compounds.

3.6. FT-IR analysis

Fig. 7 shows FTIR spectra for C1, C2, C3 and C4 samples. The peaks around 1628 and 3421 cm^{-1} correspond to the bending vibrations of absorbed water and stretching vibrations of –OH groups, respectively [26]. All FTIR spectra show absorption band at 3400 cm^{-1} corresponding to Sn–OH group. The peak at 602 cm^{-1} was attributed to terminal oxygen vibration of Sn–OH, while peak appearing at 798 cm^{-1} is due to the O–Sn–O bridge functional group of SnO_2. The strong peak near 798 cm^{-1} agrees with the stretching vibrations of Sn–O bonds and confirms that the products are well crystallized [27].

3.7. Raman spectral analysis

In order to confirm the substitution of La and its effect on the vibrational properties, Raman spectroscopy measurements were carried out. Fig. 8 shows the Raman spectra of undoped and La-doped sintered samples. Undoped SnO_2 shows prominent Raman peaks at 366 cm^{-1} and 1383 cm^{-1} which are assigned to E_g (translational) and B_{2g} (asymmetric Sn–O stretching) vibration modes of SnO_2, respectively. Raman

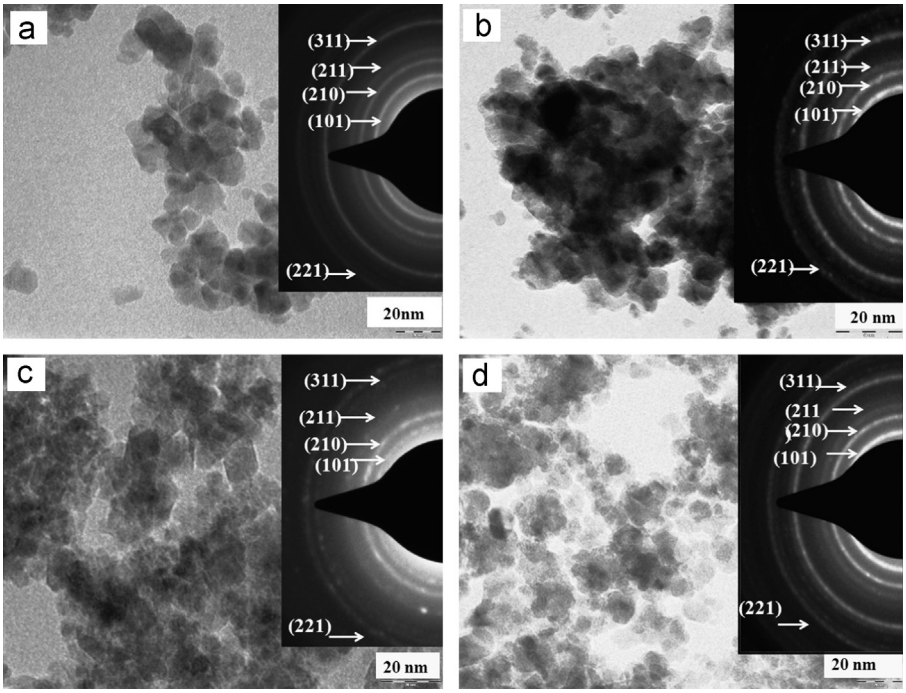

Fig. 5. TEM images with SAED patterns of SnO_2 thick films: (a) undoped SnO_2, (b) 1 mol% La doped SnO_2, (c) 3 mol% La doped SnO_2 and (d) 5 mol% La doped SnO_2.

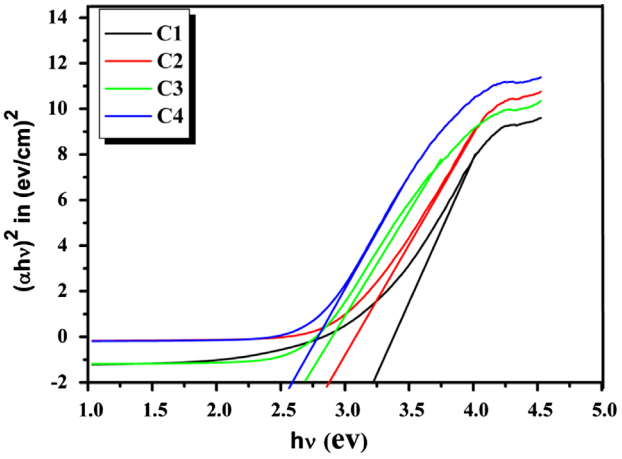

Fig. 6. The influence of La-doping on optical band gap (E_g) from the UV absorption edge of (C1) undoped SnO_2, (C2) 2 mol% La–SnO_2 and (C3) 5 mol % La–SnO_2.

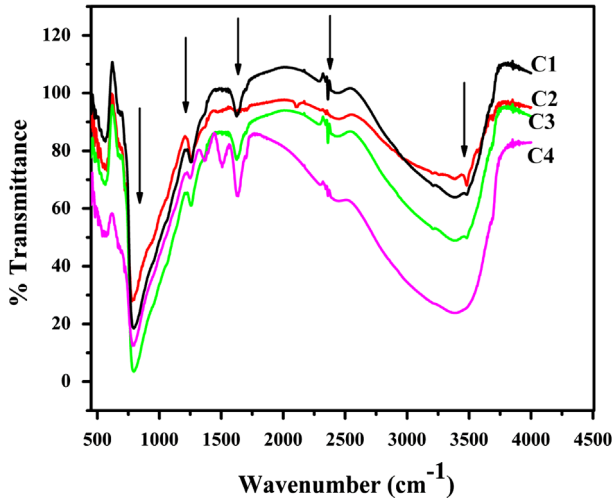

Fig. 7. FTIR spectra of (C1) undoped SnO_2, (C2) 1 mol% La, (C3) 3 mol% La and (C4) 5 mol% La doped SnO_2.

studies confirmed the tetragonal rutile structure for all SnO_2 samples [28].

3.8. Sensing properties

3.8.1. Effect of operating temperature studies

Gas sensing properties of semiconductor oxides are generally concerned with the change in the operating temperatures, mainly due to change in concentration of surface oxygen adsorbates. The response towards 2000 ppm of acetone vapor for undoped and La doped SnO_2 as a function of operating temperature is shown in Fig. 9. The undoped SnO_2 (C1) exhibits 55% response at 350 °C. On doping of 1 mol% La it increases up to 60% at 350 °C, while on further addition (3 mol%) it remarkably increases up to 96% at 300 °C. However, on further doping to 5 mol% it reduces to 70%. This indicates that 3 mol% La is an optimum concentration for getting highest response in our La doped SnO_2 system.

3.8.2. Effect of concentration

Fig. 10 shows response (S%) as a function of acetone concentration for undoped and La doped SnO_2 samples. The response is found to increase with the concentration of acetone. The response of a semiconductor metal oxide is usually depicted as $S=A[C]^N+B$, where A and B are constants and $[C]$ is the concentration of target gas or vapor; N usually has a value between 0.5 and 1.0, depending on the change of surface species and stoichiometry of the elementary reactions on

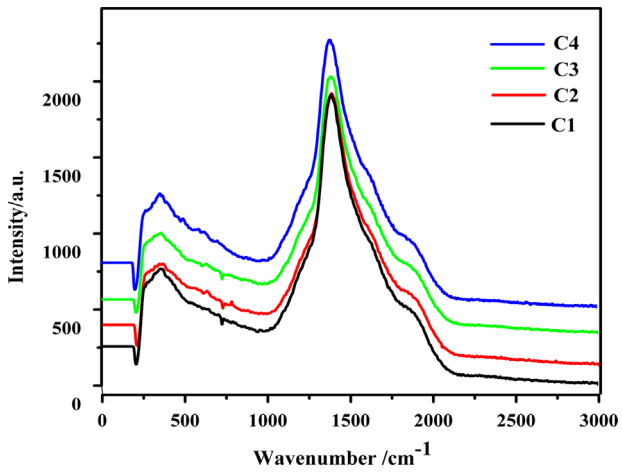

Fig. 8. Raman spectra of (C1) undoped SnO_2, (C2) 1 mol% La, (C3) 3 mol% La and (C4) 5 mol% La doped SnO_2.

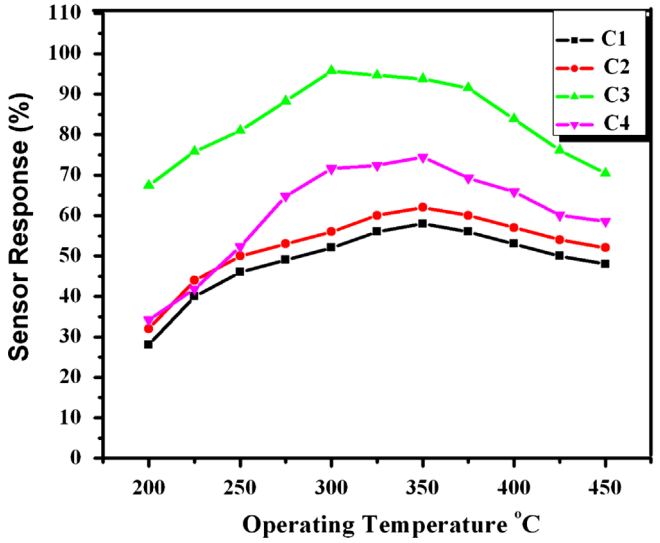

Fig. 9. Variation in sensor response towards fixed concentration of acetone vapor measured at different temperatures.

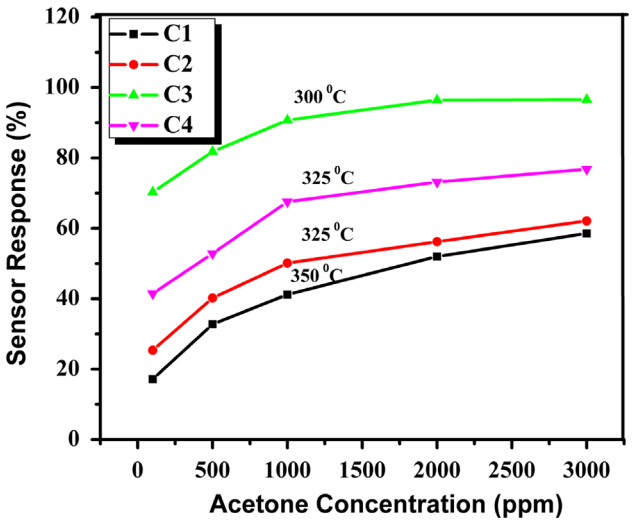

Fig. 10. Response ($S\%$) for various gases for undoped and La-doped SnO_2 at 300 °C for 100 ppm concentration of gases.

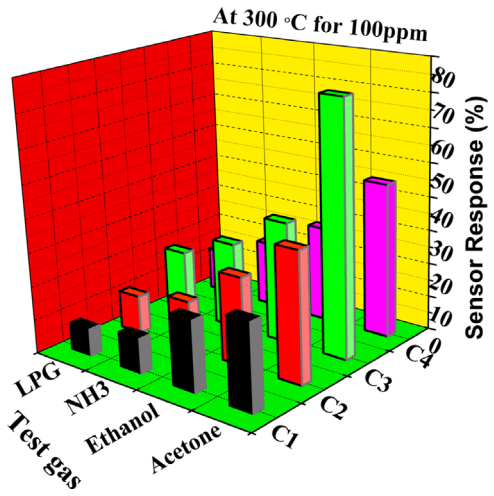

Fig. 11. Variation in response towards different concentrations of acetone vapor measured at optimal temperatures.

surface [29]. As observed from Fig. 10, there is a curvilinear relationship between response and acetone vapor concentration, indicating that $N=0.5$ for all the samples.

In view of an application as a sensor, selectivity is a major parameter. To confirm the selectivity, responses of C1, C2, C3 and C4 towards various test gases at 100 ppm concentration were studied at an operating temperature of 300 °C. It was observed (Fig. 11) that all the samples show excellent response and selectivity towards acetone vapor in comparison to other test gases. The sample C3 shows 70% response towards 100 ppm acetone which is almost three times larger than that exhibited by C1 (25%). Thus C3 sample has proved to be the potential candidate for acetone vapor detection at low concentration and at the moderate operating temperature of 300 °C.

3.8.3. Gas sensing mechanism

It is well known that gas sensing is a surface phenomenon and is mainly controlled by the amount of adsorbed oxygen species. Doping of La in SnO_2 provides oxygen deficient sites useful for the adsorption of oxygen. When such a film is heated at higher temperature, oxygen is adsorbed on the surface which abstracts electron from the conduction band thereby increasing resistance. The oxygen is adsorbed in various forms of ionic species like O^{2-}, O_2^- and O^-. The adsorption–desorption of oxygen causes a change in the Fermi level of grains and hence changes grain boundary potential barrier [30]. The reactions occurring on the surface of a sensor can be represented as follows:

$$O_{2\ (gas)} \rightarrow O_{2\ (ads)} \quad (4)$$

$$O_{2\ (ads)} + e^- \rightarrow O_{2\ (ads)}^- \quad (5)$$

$$O_{2\ (ads)}^- + e^- \rightarrow 2O^-_{\ (ads)} \quad (6)$$

$$O^-_{\ (ads)} + e^- \rightarrow O^{2-}_{\ (ads)} \quad (7)$$

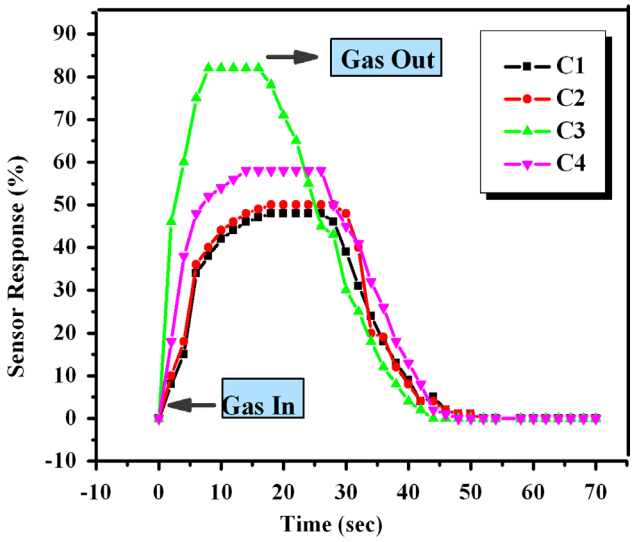

Fig. 12. Transient response characteristics of undoped SnO_2 and of various mol% La: SnO_2 exposed to 100 ppm acetone vapor at 300 °C operating temperatures.

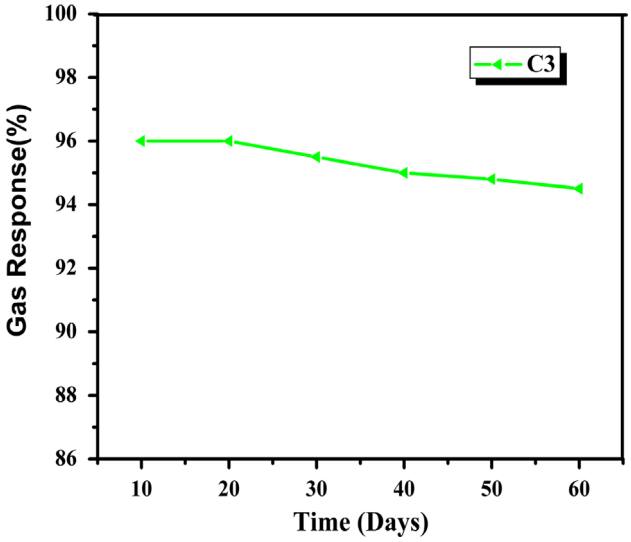

Fig. 13. Plot of stability graph of sample C3.

When SnO_2 based sensor is exposed to acetone vapor, the interaction of acetone vapor with the surface chemisorbed oxygen takes place. The reaction can be represented as follows [31]:

$$CH_3COCH_{3\ (vapor)} + 8O^-_{\ (ads)} \rightarrow 3CO_2 + 3H_2O + 8e^- \quad (8)(8)$$

This interaction results in the release of trapped electrons, thereby increasing the electron carrier concentration in conduction band of SnO_2 and hence the resistance of sensor decreases in the presence of reducing gas.

3.8.4. Transient response studies

Fig. 12 shows the response towards acetone vapor as a function of time for different SnO_2 samples. All sensors show fast response and recovery towards acetone vapor. Moreover, one can observe that sample C3 exhibits fast response and quick recovery time as compared with the other samples. It is observed that addition of La has significantly enhanced selectivity and response towards acetone. The 3 mol% La doped SnO_2 (C3) is found to be a prominent candidate for acetone sensor related applications.

3.8.5. Stability and repeatability

Stability of 3 mol% La doped SnO_2 (C3) was measured by repeating the response measurement for a number of times. The response (Fig. 13) of C3 sensor towards acetone was measured on 10th, 20th, 30th, 40th, 50th and 60th days after the first measurement. It was found that after two months, the material exhibited 97% of its earlier performance confirming the stability and reliability of sensor material for commercial application.

4. Conclusions

The undoped and La-doped SnO_2 sensors were successfully synthesized by co-precipitation method and studied for the detection of acetone vapor. The XRD and TEM studies confirmed the nanocrystallinity of the material with no impurity phases. The structural and morphological properties were strongly influenced by incorporation of La in SnO_2. The gas response studies indicated that 3 mol% La-doped SnO_2 sensor exhibits highest response with optimal operating temperature of 300 °C. The 3 mol% La doped SnO_2 appears to be a promising candidate for acetone gas sensor.

Acknowledgments

All the authors gratefully acknowledge DAE-BRNS, India for the financial support. One of the authors, J.Y. Patil, acknowledges DAE-BRNS for the grant of JRF. Dr. I.S. Mulla is grateful to CSIR, India for granting Emeritus Scientist Scheme. Authors acknowledge the SAIF—IIT Bombay for providing the TEM facility.

References

[1] X. Lou, C. Peng, X. Wang, W. Chu, Gas-sensing properties of nanostructured SnO_2-based sensor synthesized with different methods, Vacuum 81 (2007) 883–889.
[2] Z. Jie, H. Hua, G. Shan, Z. Hui, Z.J. Gui, Alcohols and acetone sensing properties of SnO_2 thin films deposited by dip-coating, Sensors and Actuators B 115 (2006) 460–464.
[3] D. Haridas, A. Chowdhuri, K. Sreenivas, V. Gupta, Effect of thickness of platinum catalyst clusters on response of SnO_2 thin film sensor for LPG, Sensors and Actuators B 153 (2011) 89–95.
[4] Z. Jiang, Z. Guo, B. Sun, Y. Jia, M. Li, J. Liu, Highly sensitive and selective butanone sensors based on cerium-doped SnO_2 thin films, Sensors and Actuators B 145 (2010) 667–673.
[5] T.D. Senguttuvan, R. Rai, S.T. Lakshmikumar, Gas sensing properties of lead doped tin oxide thick films, Materials Letters 61 (2007) 582–584.
[6] H. Miao, C. Ding, H. Luo, Antimony-doped tin dioxide nanometer powders prepared by the hydrothermal method, Microelectronic Engineering 66 (2003) 142–146.
[7] Z. Wang, L. Liu, Synthesis and ethanol sensing properties of Fe-doped SnO_2 nanofibers, Materials Letters 63 (2009) 917–919.
[8] M.D. Cabezas, D.G. Lamas, R.E. Baby, E. Cabanilla, N.E. Walsoe, Nanostructured thick film sensors for CO based on Al doped SnO_2, Journal of the Argentine Chemical Society 93 (1–3) (2005) 69–74.

[9] T. Rui-qin, G. Yan-qun, Z. Jun-hua, L. Yue, X. Tie-feng, Synthesis, characterization and gas-sensing properties of Pd-doped SnO_2 nanoparticles, Transactions of Nonferrous Metals Society 21 (2011) 1568–1573.
[10] W. Zenga, T. Liua, D. Liua, E. Han, Hydrogen sensing and mechanism of M-doped SnO_2 ($M=Cr^{3+}$, Cu^{2+} and Pd^{2+}) nanocomposite, Sensors and Actuators B 160 (2011) 455–462.
[11] Y.J. Chen, L. Nie, X.Y. Xue, Y.G. Wang, T.H. Wang, Linear ethanol sensing of SnO_2 nanorods with extremely high sensitivity, Applied Physics Letters 88 (2006) 083105.
[12] W.U. Shide, L.I. Chao, W. Wei, W.G. Huanxin, S. Yanliang, Z. Youqi, L.U. Lingzhen, Nd-doped SnO_2: characterization and its gas sensing property, Journal of Rare Earths 28 (1) (2010) 171–173.
[13] M.M. Bagheri-Mohagheghi, N. Shahtahmasebi, M.R. Alinejad, A. Youssefi, M. Shokooh-Saremi, Fe-doped SnO_2 transparent semiconducting thin films deposited by spray pyrolysis technique: thermoelectric and p-type conductivity properties, Solid State Sciences 11 (2009) 233–239.
[14] Z. Jiang, Z. Guo, B. Sun, Y. Jia, M. Li, J. Liu, Highly sensitive and selective butanone sensors based on cerium-doped SnO_2 thin films, Sensors and Actuators B 145 (2010) 667–673.
[15] Y. Niti, V. Patama, P.V. Voranipit, S. Pachara, Sinterability and microstructure of Bi-added SnO_2 nanomaterials by precipitation method, Journal of Metals, Materials and Minerals 20 (3) (2010) 67–72.
[16] H.T. Feng, R.F. Zhuo, J.T. Chen, D. Yan, J.J. Feng, H.J. Li, S. Cheng, P.X. Yan, Axial periodical nanostructures of Sb-doped SnO_2 grown by chemical vapor deposition, Physica E 41 (2009) 1640–1644.
[17] M.Y. Kim, Y.N. Choi, J.M. Bae, T.S. Oh, Carbon dioxide sensitivity of La doped thick film tin oxide gas sensor, Ceramics International 38S (2012) S657–S660.
[18] I.T. Weber, A. Valentini, L.D. Fernando, E. Longo, E.R. Leite, Catalytic activity of nanometric pure and rare earth-doped SnO_2 samples, Materials Letters 62 (2008) 1677–1680.
[19] D.R. Patil, L.A. Patil, P.P. Patil, Cr_2O_3-activated ZnO thick film resistors for ammonia gas sensing operable at room temperature, Sensors and Actuators B 126 (2007) 368–374.
[20] L.K. Bagal, J.Y. Patil, I.S. Mulla, S.S. Suryavanshi, Influence of Pd-loading on gas sensing characteristics of SnO_2 thick films, Ceramics International 38 (2012) 4835–4844.
[21] G.T. Ang, G.H. Toh, M.Z.A. Bakar, A.Z. Abdullah, M. Othman, High sensitivity and fast response SnO_2 and La SnO_2 catalytic pellet sensors in detecting volatile organic compounds, Process Safety and Environmental Protection 89 (2011) 186–192.
[22] X. Chu, X. Zhu, Y. Dong, X. Ge, S. Zhang, W. Sun, Acetone sensors based on La^{3+} doped ZnO nano-rods prepared by solvothermal method, Journal of Materials Science and Technology 28 (3) (2012) 200–204.
[23] S. Majumder, Synthesis and characterization of SnO_2 films obtained by a wet chemical process, Materials Science—Poland 27 (1) (2009) 123–129.
[24] A. Azam, A.S. Ahmed, S.S. Habib, A.H. Naqvi, Effect of Mn doping on the structural and optical properties of SnO_2 nanoparticles, Journal of Alloys and Compounds 523 (2012) 83–87.
[25] P.S. Raghupathi, J. George, C.S. Menon, The effect of substrate temperature e on electrical and optical properties of reactively evaporated tin oxide thin films, Indian Journal of Pure and Applied Physics 43 (2005) 620–623.
[26] F. Liu, B. Quana, Z. Liu, L. Chen, Surface characterization study on SnO_2 powder modified by thiourea, Materials Chemistry and Physics 93 (2005) 301–304.
[27] G. Korotcenkov, L.B. Gulina, B.K. Cho, S.H. Han, V.P. Tolstoy, SnO_2–Au nanocomposite synthesized by successive ionic layer deposition method: characterization and application in gas sensors, Materials Chemistry and Physics 128 (2011) 433–441.
[28] S.K. Pillai, L.M. Sikhwivhilu, T.K. Hillie, Synthesis, characterization and photoluminescence properties of Dy^{3+}-doped nano-crystalline SnO_2, Materials Chemistry and Physics 120 (2-3) (2009) 619–624.
[29] D. Liu, T. Liu, H. Zhang, C. Lv, W. Zeng, J. Zhang, Gas sensing mechanism and properties of Ce-doped SnO_2 sensors for volatile organic compounds, Materials Science in Semiconductor Processing 15 (4) (2012) 438–444.
[30] M.M. Rahman, A. Jamal, S.B. Khan, M. Faisal, Highly sensitive ethanol chemical sensor based on Ni-doped SnO_2 nanostructure, Biosensors and Bioelectronics 28 (2011) 127–134.
[31] L.A. Patil, M.D. Shinde, A.R. Bari, V.V. Deo, Highly sensitive ethanol sensors based on nanocrystalline SnO_2 thin films, Current Applied Physics 10 (2010) 1249–1254.